LETTER

Flexible Self-Charging, Ultrafast, High-Power-Density Ceramic Capacitor System

Mahesh Peddigari,[+] Jung Hwan Park,[+] Jae Hyun Han,[+] Chang Kyu Jeong, Jongmoon Jang, Yuho Min, Jong-Woo Kim, Cheol-Woo Ahn, Jong-Jin Choi, Byung-Dong Hahn, Sang Yeong Park, Woon-Ha Yoon, Dong-Soo Park, Dae-Yong Jeong, Jungho Ryu,* Keon Jae Lee,* and Geon-Tae Hwang*

Read Online

ACCESS | 　📊 Metrics & More | 　📰 Article Recommendations | 　🆂🅸 Supporting Information

ABSTRACT: Flexible self-charging capacitor systems, which exhibit the combined functions of energy generation and storage, are considered a promising solution for powering flexible self-powered electronics. Here, we present a new approach to demonstrate a flexible self-charging, ultrafast, and high-power-density (SUHP) capacitor system by integrating an aerosol-deposited nanograined relaxor ferroelectric $Pb(Mg_{1/3}Nb_{2/3})O_3-PbTiO_3$ (PMN−PT) capacitor and piezoelectric $Pb(Zr_x,Ti_{1-x})O_3$ (PZT) harvester. The as-designed flexible SUHP capacitor system can generate electric energy with an open-circuit voltage of 172 V and a short-circuit current of 21 μA under a biomechanical bending force of human fingers. This energy can be stored in the integrated flexible capacitor part and then discharged with a high energy density of 2.58 J/cm^3 within an ultrafast time of 480 ns. Moreover, a high power density of 5.38 MW/cm^3 from the flexible SUHP capacitor suggests that the proposed approach for self-charging and energy storage may be an efficacious way to drive future flexible pulsed-power electronic devices.
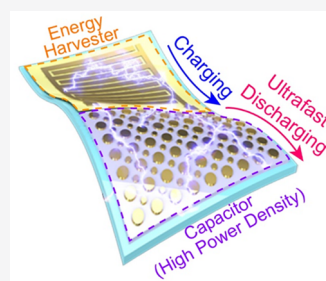
Flexible all-in-one energy conversion and storage systems have been studied by many research teams, as they can harvest electric energy from ambient mechanical and vibrational movements by a piezoelectric or triboelectric nanogenerator (PNG or TENG) and store the energy in an electrochemical cell.[1−7] By integrating the energy harvesting and energy storage devices, the self-charging power systems were demonstrated for driving self-powered miniaturized health monitoring bioelectronics and wearable smart electronics.[8−16] Various mechanisms have been demonstrated for self-powered systems, such as utilizing hybridization of energy conversion and storage devices,[1] textiles,[2] thin-film-based energy harvesters,[17,18] engineered electrodes,[13,19] conducting fabric mixed nanocomposites,[20,21] stretchable microcapacitor arrays,[22] biological cells,[23,24] and so on. State-of-the-art, flexible self-charging devices, demonstrated by scavenging ambient mechanical energy and storing the energy electrochemically, successfully stored the self-powered energy and stably discharged direct current (DC) output with large energy density. However, their unsatisfactory low output power density, slow charging/discharging process, energy conversion efficiency, and bulky complex structures impede application to future pulsed-power systems related to implantable biomedical applications (e.g., pacemakers, cardioverter defibrillators), high-power lasers, and radars.[25]

On the other hand, dielectric ceramic-based energy storage capacitors with a high dielectric constant (ε_r) and superior polarization properties can offer much higher power density because of their extremely fast discharging rates and are particularly suitable for powering pulsed-power devices.[26,27] In particular, relaxor ferroelectric (RFE) ceramics based on $Pb(Mg_{1/3}Nb_{2/3})O_3-PbTiO_3$ (PMN−PT) have garnered attention, since the polar nanoregions (PNRs) in the RFEs significantly alleviate the cooperative coupling of ferroelectric domains,[28,29] resulting in restricted spontaneous polarization and thereby narrow charge−discharge hysteresis to enable high-energy-storage efficiency.

Furthermore, the slim hysteresis loop of a ceramic dielectric is attributed to the nanosized grains that can be produced by a mechanical coating process.[30−32] Aerosol deposition (AD) can offer fast and cost-effective deposition of high-quality dense ceramic-based ferroelectric thick films.[33] This technique is favorable for the fabrication of ceramic thick films compared to conventional sol−gel coating, which requires tedious multiple repetitions of both spin coating and annealing of each thin layer to minimize cracking of the film caused by excessive
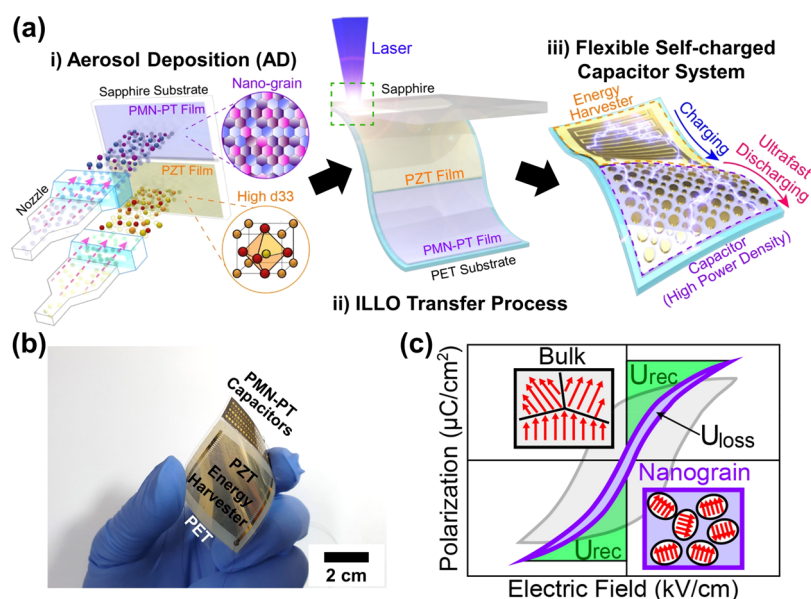
Figure 1. (a) Fabrication of the flexible self-charging, ultrafast, and high-power-density (SUHP) capacitor system. (i) Schematic illustration for deposition of high-quality PZT and PMN−PT thick films on a sapphire substrate by AD. (ii) The process of detachment of PZT and nanograined PMN−PT thick films from the sapphire substrate by using the ILLO method and transformation onto a flexible PET substrate. (iii) The final flexible SUHP capacitor system after depositing IDEs, MIMs, and a passivation layer. (b) A photograph of the SUHP capacitor system bent by human fingers to demonstrate its flexibility. (c) Schematic illustrations of typical P−E loops for large-grained and nanograined films and their corresponding energy storage properties.

tensile stress.[34] During the process, the microsized ferroelectric ceramic particles are accelerated to a nearly sonic speed (up to 300 m/s) to collide on various substrates and then form a dense film with a nanograin size (typically in the range of tens of nanometers) through the collision of primary particles.[35] Therefore, designing a flexible self-charging capacitor system by utilizing the relaxor ceramic thick film with the AD process is a potential candidate to satisfy the requirements of the above-mentioned applications due to the better recoverable energy storage efficiency and power density.

Herein, we report a self-charging, ultrafast, and high-power-density (SUHP) capacitor system by judiciously integrating an RFE capacitor with a piezoelectric harvester on a flexible plastic substrate. An aerosol-deposited flexible nanograin PMN−PT relaxor thick film was utilized as an energy storage capacitor due to its excellent-energy-charging/discharging properties. On the other hand, a flexible $Pb(Zr_xTi_{1−x})O_3$ (PZT) thick film with high piezoelectric properties was used as energy harvester to produce superior output performance for even small mechanical deformations. As a result, our flexible SUHP capacitor system generated an open-circuit voltage (V_{OC}) of 172 V and a short-circuit current of 21 μA and simultaneously stored the energy in the PMN−PT capacitor. On the discharging process, the SUHP capacitor released the stored energy with an energy density of 2.58 J/cm³ in a short time of 480 ns with a giant power density of 5.38 MW/cm³.

Figure 1a schematically illustrates the overall process for demonstrating the flexible SUHP: (i) Each PZT and PMN−PT film was individually deposited on separate sapphire substrates via the AD process at room temperature by utilizing commercially available PZT granules (average granule size of ~100 μm) and synthesized 0.9PMN−0.1PT particles. The PZT material was intentionally used for fabricating the high-performance energy harvester due to its excellent piezoelectric

properties (d_{33} up to 406 pC/N and g_{33} up to 49.5 mV/N, see Table S1 in the Supporting Information). The thickness of PZT was chosen as 7 μm to maximize its piezoelectric output performance without deteriorating film flexibility; the generated electrical energy increased proportionally to the piezoelectric layer thickness, whereas its flexibility decreased.[35] Meanwhile, the AD PMN−PT film (deposition thickness of 4.5 μm) was employed for a high energy density and ultrafast discharging capacitor because of its relaxor properties. In addition, a slim P−E curve with large saturation polarization characteristics could be produced by nanosized PMN−PT grains, which were realized through the intensive bombarding interaction between PMN−PT particles and a sapphire substrate during the AD process. Those aerosol-deposited PZT and PMN−PT films were subsequently annealed for 2 h at optimized temperatures of 900 and 500 °C, respectively, to enhance their piezoelectric and ferroelectric properties by grain growth and crystallization. (ii) Second, an inorganic-based laser lift-off (ILLO) process was carried out for transferring both of the crystallized ceramic films from the sapphire wafers onto a single polyethylene terephthalate (PET) polymer substrate. Each PZT and PMN−PT layer on an individual sapphire wafer (areas of 3.5 × 3.2 and 1 × 3.5 cm², respectively) was attached to the PET substrate (thickness of 125 μm) by using a polyurethane (PU) adhesive.[36] For the ILLO process, a 308 nm wavelength excimer (XeCl) laser was irradiated from the backside of the mother sapphire wafer. A laser beam with a moderate level (4.03 eV) of photon energy passed through the transparent sapphire (band gap of 10 eV) and then was absorbed by the bottom surface of the PZT and PMN−PT material (band gap energy of 3.3 and 3.6 eV, respectively).[37] As a result, the interfacial adhesion between the ceramic layer and sapphire substrate was drastically weakened by local vaporization interaction, allowing the PZT and PMN−PT films to be safely detached from the sacrificial
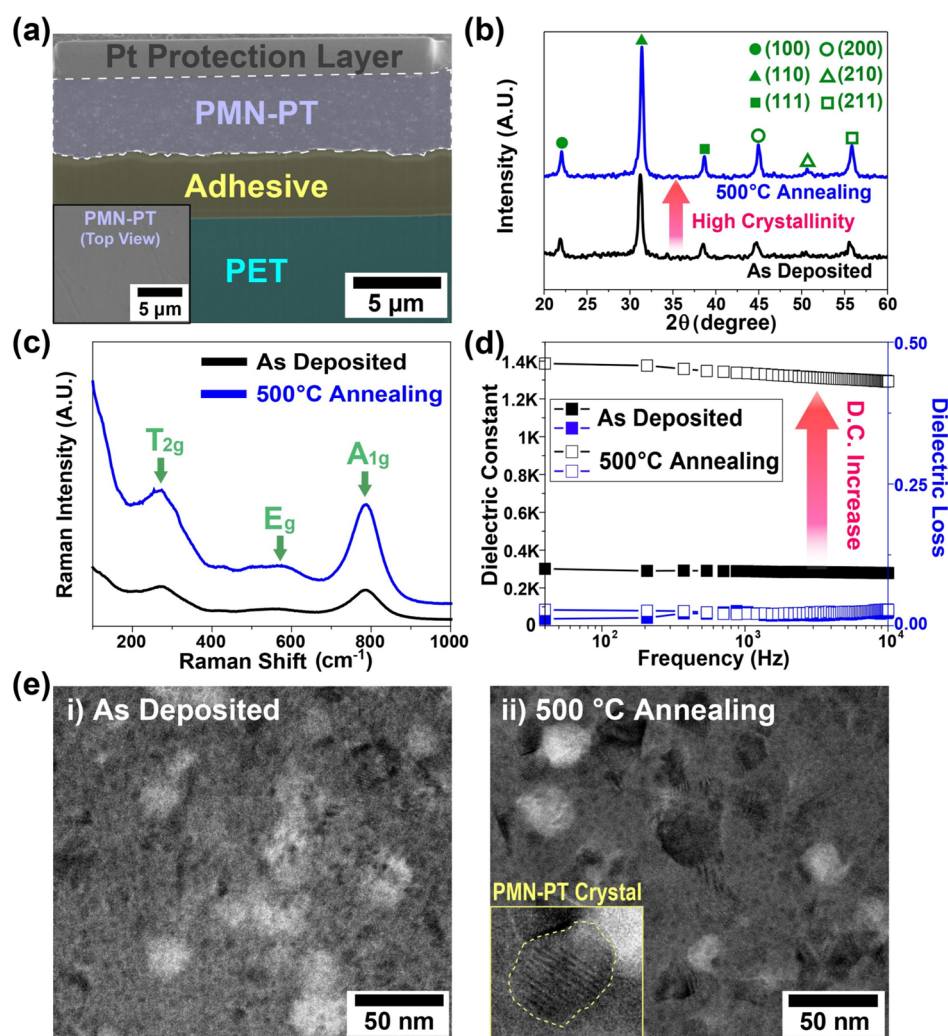
Figure 2. (a) SEM cross-sectional and surface (inset) micrographs of the PMN−PT thick film on a PET substrate deposited by AD. (b) XRD patterns, (c) Raman graphs, and (d) frequency-dependent dielectric properties of as-deposited and annealed (at 500 °C) PMN−PT thick films. The HRTEM images of (e-i) as-deposited and (e-ii) annealed (at 500 °C) PMN−PT thick films. The shaded area in the inset of (e-ii) represents the PMN−PT nanocrystal.

sapphire without any physical cracks or deformations.[38] Note that this ILLO process provided simple and stable strategies for excellent-quality inorganic layers on a large-area plastic by enabling the transfer of entire piezoelectric films on sapphire that were initially annealed at high temperature.[39] (iii) Lastly, Au interdigitated electrodes (IDEs) and metal−insulator−metal (MIM) electrodes were deposited on the flexible PZT and PMN−PT layers, respectively, to demonstrate a SUHP capacitor system on a PET, which was subsequently passivated by a photocurable PU epoxy for mechanical and electrical protection. After the device fabrication step, the flexible energy harvester was subjected to a poling process by applying an electric field of 7 kV mm^{-1} at 70 °C for 3 h to maximize the piezoelectric properties of the PZT material. The final flexible SUHP capacitor device on a plastic substrate could be operated by slightly bending the entire flexible electronic system. During the bending motion, the generated piezo-electric potential of the high-performance PZT energy harvester could produce electric power to sufficiently charge the PMN−PT capacitor. The stored electrical energy could be discharged in an extremely fast manner by a high-energy

density capacitor, which was enabled via the nanograin induced relaxor ferroelectric property.

Figure 1b shows a photographic image of the final flexible SUHP capacitor system on a single plastic substrate bent by human fingers. Lateral-type Au IDEs on the flexible PZT layer had a total area of 2.5 × 3 cm^2, an electrode width of 90 μm, an electrode interdistance of 100 μm, a finger length of 2.4 cm, and 70 finger pairs. The PMN−PT capacitors had circle-shaped top electrodes (diameter of 500 μm) and a whole-area-coated bottom electrode (Cr/Au/Ag/ITO) (see Figure S1 in the Supporting Information). In general, the relaxor behavior in ferroelectric materials is caused by the destruction of long-range ordering on ferroelectric domains and by the formation of PNRs.[29,40] The PNRs originate from the inherent charge and structural inhomogeneity in the relaxor with the introduction of defect dipoles in the unit cell of ferroelectric materials. Moreover, this behavior could be possible by depositing a ferroelectric film of nanosized grains using the AD process with maintenance of the initial bulk composition.[30] Figure 1c presents a schematic diagram of typical P−E curves for ferroelectric bulk and AD films. The nanocrystalline AD ceramic film could have a relatively slim P−E loop with higher
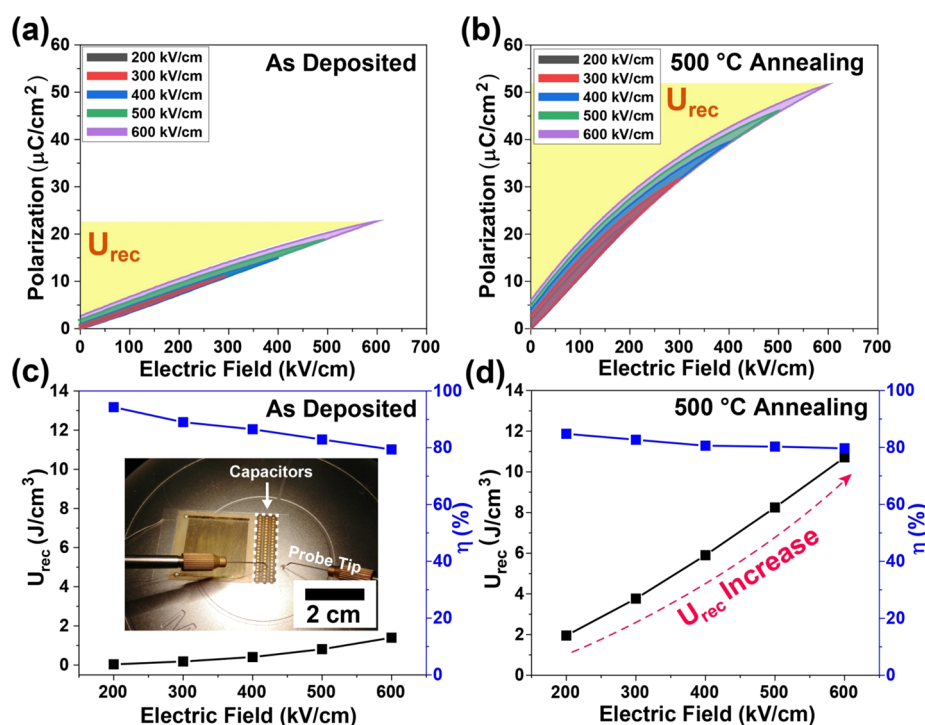
Figure 3. P–E loops of (a) as-deposited and (b) annealed PMN–PT thick films measured at various electric fields from 200 to 600 kV/cm. The estimated energy storage properties of (c) as-deposited and (d) annealed PMN–PT thick-film capacitors. The inset of (c) shows a photograph of the P–E measurement for the flexible PMN–PT thick-film SUHP capacitor.

recoverable energy density (U_{rec}) and lower energy loss (U_{loss}) compared to the bulk ceramic, which would be beneficial to demonstrate a high-performance pulsed-power capacitor.

Figure 2a shows a cross-sectional scanning electron microscopy (SEM) image of the AD PMN–PT thick film on the plastic substrate after the ILLO process. A focused ion beam (FIB) was utilized as a milling cutter to form the cross-sectional device plane. Since the FIB process could produce a damaged layer on the PMN–PT film, the Pt deposition was used as a protection layer for subsequent milling for cross-section sample preparation.[41] The PMN–PT was bonded on the PU adhesive layer without mechanical damage such as blisters and cracks in the AD ceramic film. The highly dense microstructure of the PMN–PT film originated from the effective arrangement of the fractured and deformed ceramic particles during the AD process. The bottom electrode layers under PMN–PT were very thin (the thicknesses of Cr, Au, and ITO were <10, ~100, and ~130 nm, respectively) compared with other layers of PMN–PT (~4.5 μm), adhesion (~3.8 μm), and PET (~125 μm). Therefore, the bottom electrode layers of SUHP were not distinctly presented in the cross-sectional SEM image. Figure 2b presents X-ray diffraction (XRD) patterns of as-deposited and postannealed flexible PMN–PT films, which show that the PMN–PT samples have a crystallized phase with pure perovskite peaks without any pyrochlore or other second phases. Raman spectroscopy was performed, as shown in Figure 2c, to examine the phases of the as-deposited and annealed PMN–PT samples by utilizing a 514.5 nm Ar$^+$ ion laser. Both PMN–PT films exhibited similar Raman modes located at around 270, 550, and 800 cm^{-1}, which correspond to the T_{2g}, E_g, and A_{1g} modes, respectively, in good agreement with typical overlapped tetragonal and rhombohedral phases with a perovskite structure.[42] It is believed that the PNRs in the

rhombohedral phase induce relaxor behavior, while the normal microscale domains in the tetragonal phase exhibit ferroelectric behavior.[42] In the case of the as-deposited PMN–PT film, all the XRD peaks and Raman modes were broad owing to the smaller crystallite sizes as well as the highly disordered crystallinity, since an amorphous phase could be formed by the particle fracture during high-kinetic-energy collisions in the AD process. After annealing the PMN–PT film, the intensity of the XRD peaks and Raman modes increased, and the corresponding full width at half maximums were reduced (see Figure S2 in the Supporting Information for PZT film), implying enhanced crystallinity of the ferroelectric material.[32] To achieve a high energy density for a capacitor, the ferroelectric should have a high dielectric constant (ε_r) and low dielectric loss (tan δ). Figure 2d shows the frequency dependence of ε_r and tan δ of the flexible PMN–PT thick films in the range of 40 Hz to 10 kHz. The annealed sample displayed higher values of ε_r (1335 at 1 kHz) and tan δ (2.3% at 1 kHz) as compared to the as-deposited sample (288 and 2.1% at 1 kHz, respectively). The higher ε_r of the annealed PMN–PT film can be correlated to relatively improved crystallinity and a larger crystallite size, which may promote domain wall motion in the ferroelectric material. In order to observe nanostructures, the as-deposited and annealed PMN–PT films were examined by high-resolution transmission electron microscopy (HRTEM), as shown in Figure 2e. From the lattice images and selected area electron beam diffraction patterns (see Figure S3 in the Supporting Information), it is clear that the as-deposited PMN–PT film has a nearly amorphous structure (Figure 2e-i), while the film annealed at 500 °C has a noticeably increased number of nanocrystalline phases (Figure 2e-ii). Therefore, the annealing process at a relatively low temperature for PMN–PT induced growth of nanosize crystals rather than microscale grains, which could significantly enhance RFE properties while

maintaining the narrow $P-E$ hysteresis loop.[30] The energy dispersive spectrum results indicated that all elements were present in the nanograined PMN−PT annealed film (see Figure S4 in the Supporting Information).

To obtain the energy storage properties such as U_{rec} and energy storage efficiency (η) of the flexible PMN−PT thick-film capacitors for the as-deposited films and the films annealed at 500 °C, the polarization−electric field ($P-E$) hysteresis loops were measured under a unipolar electric field with increasing peak field and estimated using the following the equations[26,27]

$$U_{rec} = \int_{P_r}^{P_{max}} E dP \tag{1}$$

$$\eta = \frac{U_{rec}}{U_{rec} + U_{loss}} \tag{2}$$

where P_{max} is the maximum polarization, P_r is the remnant polarization, E is the applied electric field, and U_{loss} is the energy loss that is derived by the closed area of $P-E$ hysteresis loop. From eqs 1 and 2, the capacitive material requires a high dielectric constant (ε_r) or P_{max}, low P_r, high dielectric breakdown strength (E_b), and slimmed polarization hysteresis curve to maximize the U_{rec} and η properties. Here, the $P-E$ loops for both as-deposited and annealed PMN−PT thick-film capacitors were measured from 200 to 600 kV/cm to estimate the energy storage properties, because the annealed film exhibited a maximum E_b of 600 kV/cm. Both PMN−PT films exhibited slim hysteresis loops with low remnant polarizations. The as-deposited PMN−PT capacitor shows a paraelectric-like hysteresis curve with small values of P_{max} (∼22.6 μC/cm^2) and P_r (∼2.6 μC/cm^2) at an applied electric field of 600 kV/cm. In contrast, the annealed sample shows an RFE-like ferroelectric hysteresis curve with an improved P_{max} of 51.6 μC/cm^2 and P_r of 6.3 μC/cm^2 as presented in Figure 3a,b. The as-deposited flexible PMN−PT exhibited weak ferroelectric hysteresis, but the high-temperature annealing process recovered the ferroelectric property, which was derived by the enhanced crystallinity of the PMN−PT material. The difference in P_{max} and P_r (i.e., $P_{max} - P_r$) was greatly increased with the annealing procedure (20.0 μC/cm^2 for the as-deposited film and 45.3 μC/cm^2 for the 500 °C annealed film), thus improving the energy storage density. Figure 3c,d shows U_{rec} and η depending on the applied electric fields for the as-deposited and annealed PMN−PT films. The inset of Figure 3c presents a photograph of the $P-E$ measurement of a flexible capacitor. The U_{rec} values of the as-deposited and annealed samples were 1.4 and 10.7 J/cm^3, respectively, at an applied electric field of 600 kV/cm, and thus, the annealing process enabled a dramatic ∼7.6 times enhancement of U_{rec} compared to the pristine case. This energy density is much higher than the values of previously reported polymer-based flexible capacitors at an electric field of 600 kV/cm.[43,44] Additionally, the annealed flexible PMN−PT had a stable η as a function of the electric field from 200 (η of 84.8%) to 600 kV/cm (η of 79.7%), while the as-deposited film showed a relatively high decline of η with increment of the electric field (η of 94.3% at 200 kV/cm and 79.4% at 600 kV/cm). The dense microstructure with more nanograins of annealed PMN−PT could result in a large number of grain boundaries with better conduction loss at high electric fields.[30] Further, the most probable dielectric breakdown field (or characteristic E_b) of the annealed PMN−PT film capacitor was

estimated using the two-parameter Weibull distribution (see Supporting Information).[26] The statistical values of E_b were obtained, and the E_b distribution was fitted to the Weibull distribution as shown in Figure S5. The PMN−PT thick-film capacitor exhibited a characteristic E_b of 505 kV/cm with a Weibull modulus of 3.50.

To utilize the flexible high-storage-density capacitors in pulsed-power and high-power applications, high energy density with a short discharge time is required. The discharge energy density and discharge time ($\tau_{0.9}$) of the PMN−PT films were characterized by a static charge−discharge method using a high-speed switching circuit.[30] Here, $\tau_{0.9}$ is defined as the time needed for 90% discharging of stored energy of the flexible capacitor. Figure 4a shows the circuit diagram for the measurement of the charge−discharge properties of the flexible PMN−PT capacitor. The detailed procedure of the static charge−discharge method is described as follows:[45] (i) the PMN−PT capacitor is charged by the direct current (DC) high-voltage source. (ii) The PMN−PT capacitor then discharges the voltage across a load resistance as a power
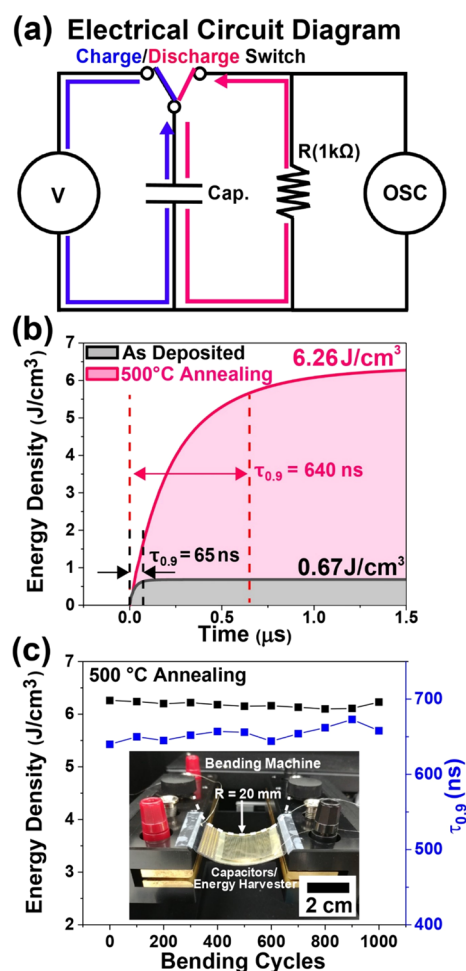

Figure 4. (a) Schematic diagram of charging−discharging measurement system. (b) The time-domain profiles of discharged energy density of as-deposited and annealed (at 500 °C) PMN−PT thick-film capacitors. (c) The performance of the flexible PMN−PT capacitor against 1000 bending/releasing cycles with a curvature radius of 20 mm. The inset displays a photograph of the flexible SUHP capacitor during the bending/releasing measurement.
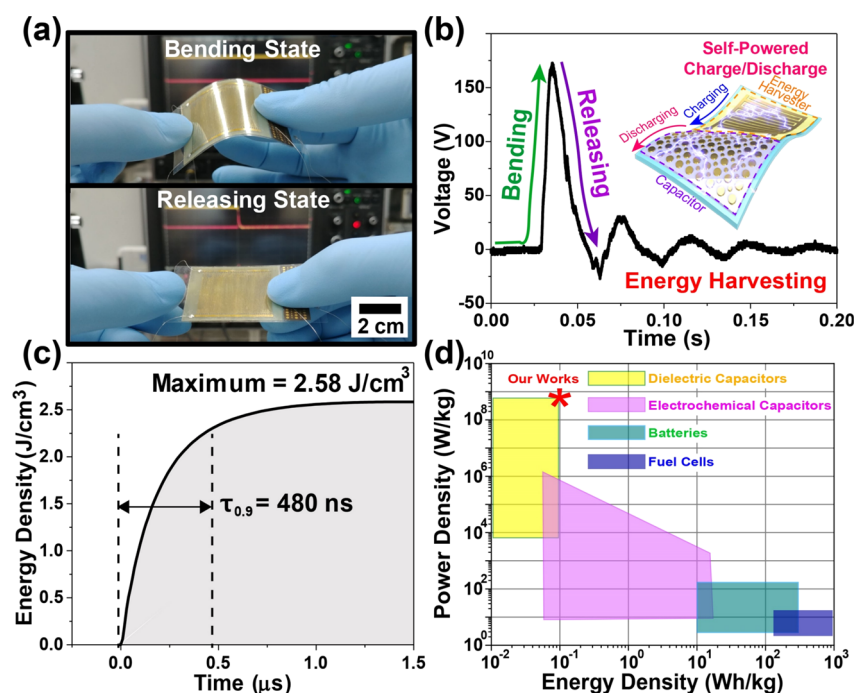
Figure 5. (a) Photograph of the integrated flexible SUHP capacitor system that scavenges the mechanical energy from biomechanical bending motion by human fingers. (b) The generated voltage and (c) discharged energy density delivered from the SUHP capacitor system under bending force by human fingers. The inset of (b) presents the operation concept of the SUHP capacitor system. (d) Ragone plot for comparing the specific energy and power densities of the SUHP capacitor with other energy storage devices.

source. (iii) The voltage signal applied on the load resistance is simultaneously recorded by an oscilloscope. As a result, we obtained the energy density curve as a function of time during the discharging process. For the measurement, the PMN−PT film capacitors were charged under an electric field of 600 kV/cm and discharged through a load resistor of 1 kΩ. For the discharging state of dielectric capacitors, a lower resistance could guarantee a faster discharging of stored electric charges in the capacitor through the external resistance (Figure S6 in Supporting Information). By this reason, the discharging performance of previously reported dielectric capacitors was also characterized with the relatively low resistances such as 100 Ω, 1 kΩ, and 2 kΩ.[30,46,47] The time-dependent discharge energy density $[U_{rec} = \int V^2(t)/R \cdot dt]$ of the flexible PMN−PT capacitors was derived from the discharging profiles, where $V(t)$ is the voltage at time t and R is the external load resistance. As shown in Figure 4b, the as-deposited PMN−PT film displayed a very fast $\tau_{0.9}$ of 65 ns with a U_{rec} of 0.67 J/cm^3 at 600 kV/cm, which is faster than other capacitor films owing to the paraelectric-like behavior arising from the nanoscale crystallites embedded in the amorphous structure.[48] Meanwhile, the annealed PMN−PT film displayed $\tau_{0.9}$ and U_{rec} values of 640 ns and 6.26 J/cm^3 at 600 kV/cm, respectively. Since the discharging power density of the PMN−PT capacitor could be derived by the equation of $U_{rec}/\tau_{0.9}$, as-deposited and annealed samples presented power densities of 10.3 and 9.8 MW/cm^3, respectively. Figure 4c depicts the variation of U_{rec} and $\tau_{0.9}$ under a bending fatigue test of the annealed flexible PMN−PT capacitor with repeated bending and unbending cycles. The capacitor device retains its mechanical robustness and stability over 1000 bending motions at a curvature radius of 20 mm. In addition, the electric fatigue endurance of the flexible capacitor is also confirmed by measuring up to 10^7

electric cycles, showing no significant degradation, as presented in Figure S7 (Supporting Information).

To verify the applicability of our proposed system for powering flexible high-power devices, we demonstrated a flexible SUHP capacitor system by charging the electric energy generated from the PZT harvester into the PMN−PT capacitor and then discharging the energy through an external 1 kΩ load resistance. The working mechanism of the flexible SUHP capacitor device is an electric charge and discharge process driven by the piezoelectric potential generation as a result of displacement and redistribution of free dipoles in the harvester part under the external mechanical stimulation. Initially, the PMN−PT capacitor can be in a discharged state, and then with the bending motion of the flexible SUHP capacitor system, the piezoelectric PZT harvesting part can produce electric potential between the electrodes and meanwhile provide electric energy for charging the PMN−PT capacitor.

Prior to evaluating the self-charging performance of the flexible SUHP capacitor system, the output performance of the flexible PZT harvester was investigated by a biomechanical bending motion using human fingers as shown in Figure 5a,b. Upon application of bending force (∼1 N, see Figure S8 in the Supporting Information), the PZT harvester generated a maximum open-circuit voltage (V_{OC}) of 172 V (which corresponds to an electric field of 382 kV/cm for the PMN−PT capacitor) and a maximum short-circuit current of 21.6 μA as shown in Figure S9 (see Supporting Information). At an optimum load resistance of 10 MΩ, the estimated output energy density of the PZT harvester is approximately 1.4 mJ/cm^3 (Figure S10 in Supporting Information). The operating concept of the self-charging capacitor system is displayed in the inset of Figure 5b, which consists of the PZT harvester as the power source and the PMN−PT capacitor as the energy

storage device. The external microswitch enables either energy storage or discharge mode with a connecting load resistance of 1 kΩ. After voltage generation of about 170 V is ensured from the flexible PZT harvester by repeated bending/unbending motions, the generated electric energy was transferred instantly to the flexible PMN−PT capacitor via a high-speed microswitch. After the capacitor charged using the harvested energy, the stored energy in the PMN−PT capacitor was discharged through the load resister. Figure 5c presents the time-dependent discharging curve of the SUHP capacitor, where it quickly discharged the stored energy with a U_{rec} of 2.58 J/cm^3 and $\tau_{0.9}$ of 480 ns. The discharging power density of the SUHP capacitor is calculated as 5.38 MW/cm^3 (664.2 MW/kg since the density of PMN−PT is 8.1 g/cm^3).[49] Interestingly, the SUHP capacitor delivered manifold larger power density than flexible supercapacitors with similar energy density as well as other energy storage systems as shown in Table S2 (Supporting Information) and Figure 5d.[25,26] Moreover, compared with previously reported flexible self-charging and energy storage devices, our approach requires only a few simple steps and is feasible for a scaled-up process. The obtained results suggest that our proposed flexible SUHP capacitor system opens a new pathway to drive high-power portable and flexible smart electronics, which was enabled by a structural design that integrates a flexible high-performance piezoelectric energy harvester and an ultrafast high-power-density capacitor. In this work, we cannot present a practical demonstration for real pulsed-power devices due to a very low discharged energy from the SUHP capacitor. Since the volume of single capacitor cell under a dot-shaped top electrode was just 8.82×10^{-7} cm^3, the total discharged energy from the capacitor cell was 5.56 μJ, which was very small to conduct a practical demonstration for the pulsed-power electronics. Therefore, the cell volume of PMN−PT capacitor should be dramatically increased by an advanced capacitor manufacturing process (e.g., multilayered capacitor) to demonstrate practical pulsed-power applications.[50]

In summary, a new approach is adopted for fabricating a flexible SUHP capacitor system by coupling the nanograined dielectric PMN−PT thick film with the piezoelectric PZT thick film. The proposed energy device not only scavenges electrical energy from external mechanical movement but also stores/releases the electric energy in a quick time. It generates high electric output ($V_{OC} \approx 172$ V, $I_{max} \approx 21.6$ μA) under a biomechanical bending motion to charge the dielectric capacitor. The annealing process at 500 °C for the PMN−PT capacitor enables the stored energy to be discharged with an energy density of 2.58 J/cm^3 in a very short time ($\tau_{0.9}$ of 480 ns). Moreover, the high power density of 5.38 MW/cm^3 is recorded during the discharge operation. Outstanding performance with excellent flexibility of the as-designed SUHP capacitor suggests that this new approach provides essential progress in sustainable pulsed-power sources for driving flexible electronics.[51,52]

■ ASSOCIATED CONTENT

ⓢ Supporting Information

The Supporting Information is available free of charge at https://pubs.acs.org/doi/10.1021/acsenergylett.1c00170.

Experimental section, Figures S1−S11, and Table S1−S2 (PDF)

■ AUTHOR INFORMATION

Corresponding Authors

Geon-Tae Hwang − *Department of Materials Science and Engineering, Pukyong National University, Busan 42601, Republic of Korea;* ⓞ orcid.org/0000-0001-6151-3887; Email: gthwang@pknu.ac.kr

Keon Jae Lee − *Department of Materials Science and Engineering, Korea Advanced Institute of Science and Technology (KAIST), Daejeon 34141, Republic of Korea;* Email: keonlee@kaist.ac.kr

Jungho Ryu − *School of Materials Science & Engineering, Yeungnam University, Gyeongan, Gyeongbuk 38541, Republic of Korea;* ⓞ orcid.org/0000-0002-4746-5791; Email: jhryu@ynu.ac.kr

Authors

Mahesh Peddigari − *Department of Functional Ceramics, Korea Institute of Materials Science (KIMS), Changwon 51508, Republic of Korea*

Jung Hwan Park − *Department of Mechanical Engineering (Department of Aeronautics, Mechanical and Electronic Convergence Engineering), Kumoh National Institute of Technology, Gumi, Gyeongbuk 39177, Republic of Korea*

Jae Hyun Han − *Department of Materials Science and Engineering, Korea Advanced Institute of Science and Technology (KAIST), Daejeon 34141, Republic of Korea*

Chang Kyu Jeong − *Division of Advanced Materials Engineering, Jeonbuk National University, Jeonju, Jeonbuk 54896, Republic of Korea*

Jongmoon Jang − *Department of Functional Ceramics, Korea Institute of Materials Science (KIMS), Changwon 51508, Republic of Korea*

Yuho Min − *Department of Functional Ceramics, Korea Institute of Materials Science (KIMS), Changwon 51508, Republic of Korea;* ⓞ orcid.org/0000-0002-0784-4818

Jong-Woo Kim − *Department of Functional Ceramics, Korea Institute of Materials Science (KIMS), Changwon 51508, Republic of Korea*

Cheol-Woo Ahn − *Department of Functional Ceramics, Korea Institute of Materials Science (KIMS), Changwon 51508, Republic of Korea*

Jong-Jin Choi − *Department of Functional Ceramics, Korea Institute of Materials Science (KIMS), Changwon 51508, Republic of Korea*

Byung-Dong Hahn − *Department of Functional Ceramics, Korea Institute of Materials Science (KIMS), Changwon 51508, Republic of Korea*

Sang Yeong Park − *Hanwha Systems, Seongnam-Si, Gyeonggi-Do 13524, Korea*

Woon-Ha Yoon − *Department of Functional Ceramics, Korea Institute of Materials Science (KIMS), Changwon 51508, Republic of Korea*

Dong-Soo Park − *Department of Functional Ceramics, Korea Institute of Materials Science (KIMS), Changwon 51508, Republic of Korea*

Dae-Yong Jeong − *Department of Materials Science & Engineering, Inha University, Incheon 22212, Republic of Korea;* ⓞ orcid.org/0000-0002-6022-938X

Complete contact information is available at: https://pubs.acs.org/10.1021/acsenergylett.1c00170

Author Contributions

+M.P., J.H.P., and J.H.H. contributed equally to this work

REFERENCES

(1) Xue, X.; Wang, S.; Guo, W.; Zhang, Y.; Wang, Z. L. Hybridizing Energy Conversion and Storage in a Mechanical-to-Electrochemical Process for Self-Charging Power Cell. *Nano Lett.* **2012**, *12* (9), 5048–5054.

(2) Pu, X.; Li, L.; Song, H.; Du, C.; Zhao, Z.; Jiang, C.; Cao, G.; Hu, W.; Wang, Z. L. A Self-Charging Power Unit by Integration of a Textile Triboelectric Nanogenerator and a Flexible Lithium-Ion Battery for Wearable Electronics. *Adv. Mater.* **2015**, *27* (15), 2472–2478.

(3) Shi, X.; Chen, S.; Zhang, H.; Jiang, J.; Ma, Z.; Gong, S. Portable Self-Charging Power System via Integration of a Flexible Paper-Based Triboelectric Nanogenerator and Supercapacitor. *ACS Sustainable Chem. Eng.* **2019**, *7* (22), 18657–18666.

(4) Luo, J.; Wang, Z. L. Recent advances in triboelectric nanogenerator based self-charging power systems. *Energy Storage Mater.* **2019**, *23*, 617–628.

(5) Song, W.; Yin, X.; Liu, D.; Ma, W.; Zhang, M.; Li, X.; Cheng, P.; Zhang, C.; Wang, J.; Wang, Z. L. A highly elastic self-charging power system for simultaneously harvesting solar and mechanical energy. *Nano Energy* **2019**, *65*, 103997.

(6) Rasheed, A.; He, W.; Qian, Y.; Park, H.; Kang, D. J. Flexible Supercapacitor-Type Rectifier-free Self-Charging Power Unit Based on a Multifunctional Polyvinylidene Fluoride–ZnO–rGO Piezoelectric Matrix. *ACS Appl. Mater. Interfaces* **2020**, *12* (18), 20891–20900.

(7) Wang, Z. L.; Chen, J.; Lin, L. Progress in triboelectric nanogenerators as a new energy technology and self-powered sensors. *Energy Environ. Sci.* **2015**, *8* (8), 2250–2282.

(8) He, H.; Fu, Y.; Zhao, T.; Gao, X.; Xing, L.; Zhang, Y.; Xue, X. All-solid-state flexible self-charging power cell basing on piezo-electrolyte for harvesting/storing body-motion energy and powering wearable electronics. *Nano Energy* **2017**, *39*, 590–600.

(9) Chen, X.; Villa, N. S.; Zhuang, Y.; Chen, L.; Wang, T.; Li, Z.; Kong, T. Stretchable Supercapacitors as Emergent Energy Storage Units for Health Monitoring Bioelectronics. *Adv. Energy Mater.* **2020**, *10* (4), 1902769.

(10) Song, Y.; Wang, H.; Cheng, X.; Li, G.; Chen, X.; Chen, H.; Miao, L.; Zhang, X.; Zhang, H. High-efficiency self-charging smart bracelet for portable electronics. *Nano Energy* **2019**, *55*, 29–36.

(11) Lin, Z.; Yang, J.; Li, X.; Wu, Y.; Wei, W.; Liu, J.; Chen, J.; Yang, J. Large-Scale and Washable Smart Textiles Based on Triboelectric Nanogenerator Arrays for Self-Powered Sleeping Monitoring. *Adv. Funct. Mater.* **2018**, *28* (1), 1704112.

(12) He, T.; Wang, H.; Wang, J.; Tian, X.; Wen, F.; Shi, Q.; Ho, J. S.; Lee, C. Self-Sustainable Wearable Textile Nano-Energy Nano-System (NENS) for Next-Generation Healthcare Applications. *Adv. Sci.* **2019**, *6* (24), 1901437.

(13) Maitra, A.; Paria, S.; Karan, S. K.; Bera, R.; Bera, A.; Das, A. K.; Si, S. K.; Halder, L.; De, A.; Khatua, B. B. Triboelectric Nanogenerator Driven Self-Charging and Self-Healing Flexible Asymmetric Supercapacitor Power Cell for Direct Power Generation. *ACS Appl. Mater. Interfaces* **2019**, *11* (5), 5022–5036.

(14) Pu, X.; Hu, W.; Wang, Z. L. Toward Wearable Self-Charging Power Systems: The Integration of Energy-Harvesting and Storage Devices. *Small* **2018**, *14* (1), 1702817.

(15) Kim, J.; Lee, J.-H.; Lee, J.; Yamauchi, Y.; Choi, C. H.; Kim, J. H. Research Update: Hybrid energy devices combining nanogenerators and energy storage systems for self-charging capability. *APL Mater.* **2017**, *5* (7), 073804.

(16) Baek, C.; Yun, J. H.; Wang, J. E.; Jeong, C. K.; Lee, K. J.; Park, K.-I.; Kim, D. K. A flexible energy harvester based on a lead-free and piezoelectric BCTZ nanoparticle–polymer composite. *Nanoscale* **2016**, *8* (40), 17632–17638.

(17) Zhu, G.; Zhou, Y. S.; Bai, P.; Meng, X. S.; Jing, Q.; Chen, J.; Wang, Z. L. A Shape-Adaptive Thin-Film-Based Approach for 50% High-Efficiency Energy Generation Through Micro-Grating Sliding Electrification. *Adv. Mater.* **2014**, *26* (23), 3788–3796.

(18) Thakur, P.; Kool, A.; Hoque, N. A.; Bagchi, B.; Khatun, F.; Biswas, P.; Brahma, D.; Roy, S.; Banerjee, S.; Das, S. Superior performances of in situ synthesized ZnO/PVDF thin film based self-poled piezoelectric nanogenerator and self-charged photo-power bank with high durability. *Nano Energy* **2018**, *44*, 456–467.

(19) Tang, W.; Jiang, T.; Fan, F. R.; Yu, A. F.; Zhang, C.; Cao, X.; Wang, Z. L. Liquid-Metal Electrode for High-Performance Triboelectric Nanogenerator at an Instantaneous Energy Conversion Efficiency of 70.6%. *Adv. Funct. Mater.* **2015**, *25* (24), 3718–3725.

(20) Karan, S. K.; Bera, R.; Paria, S.; Das, A. K.; Maiti, S.; Maitra, A.; Khatua, B. B. An Approach to Design Highly Durable Piezoelectric Nanogenerator Based on Self-Poled PVDF/AlO-rGO Flexible Nanocomposite with High Power Density and Energy Conversion Efficiency. *Adv. Energy Mater.* **2016**, *6* (20), 1601016.

(21) Zhang, Y.; Zhang, Y.; Xue, X.; Cui, C.; He, B.; Nie, Y.; Deng, P.; Lin Wang, Z. PVDF–PZT nanocomposite film based self-charging power cell. *Nanotechnology* **2014**, *25* (10), 105401.

(22) Lim, Y.; Yoon, J.; Yun, J.; Kim, D.; Hong, S. Y.; Lee, S.-J.; Zi, G.; Ha, J. S. Biaxially Stretchable, Integrated Array of High Performance Microsupercapacitors. *ACS Nano* **2014**, *8* (11), 11639–11650.

(23) Wang, X.; Yin, Y.; Yi, F.; Dai, K.; Niu, S.; Han, Y.; Zhang, Y.; You, Z. Bioinspired stretchable triboelectric nanogenerator as energy-harvesting skin for self-powered electronics. *Nano Energy* **2017**, *39*, 429–436.

(24) Maitra, A.; Karan, S. K.; Paria, S.; Das, A. K.; Bera, R.; Halder, L.; Si, S. K.; Bera, A.; Khatua, B. B. Fast charging self-powered wearable and flexible asymmetric supercapacitor power cell with fish swim bladder as an efficient natural bio-piezoelectric separator. *Nano Energy* **2017**, *40*, 633–645.

(25) Amar, A. B.; Kouki, A. B.; Cao, H. Power Approaches for Implantable Medical Devices. *Sensors* **2015**, *15* (11), 28889–28914.

(26) Palneedi, H.; Peddigari, M.; Hwang, G.-T.; Jeong, D.-Y.; Ryu, J. High-Performance Dielectric Ceramic Films for Energy Storage Capacitors: Progress and Outlook. *Adv. Funct. Mater.* **2018**, *28* (42), 1803665.

(27) Peddigari, M.; Palneedi, H.; Hwang, G.-T.; Ryu, J. Linear and Nonlinear Dielectric Ceramics for High-Power Energy Storage Capacitor Applications. *Han'guk Seramik Hakhoechi* **2019**, *56* (1), 1–23.

(28) Yao, K.; Chen, S.; Rahimabady, M.; Mirshekarloo, M. S.; Yu, S.; Tay, F. E. H.; Sritharan, T.; Lu, L. Nonlinear dielectric thin films for high-power electric storage with energy density comparable with electrochemical supercapacitors. *IEEE Trans. Ultrason. Ferroelectr. Freq. Contr.* **2011**, *58* (9), 1968–1974.

(29) Cowley, R. A.; Gvasaliya, S. N.; Lushnikov, S. G.; Roessli, B.; Rotaru, G. M. Relaxing with relaxors: a review of relaxor ferroelectrics. *Adv. Phys.* **2011**, *60* (2), 229–327.

(30) Peddigari, M.; Palneedi, H.; Hwang, G.-T.; Lim, K. W.; Kim, G.-Y.; Jeong, D.-Y.; Ryu, J. Boosting the Recoverable Energy Density of Lead-Free Ferroelectric Ceramic Thick Films through Artificially Induced Quasi-Relaxor Behavior. *ACS Appl. Mater. Interfaces* **2018**, *10* (24), 20720−20727.

(31) Jung, H.-B.; Lim, J.-H.; Peddigari, M.; Ryu, J.; Choi, D. H.; Jeong, D.-Y. Enhancement of energy storage and thermal stability of relaxor Pb0.92La0.08Zr0.52Ti0.48O3-Bi(Zn0.66Nb0.33)O3 thick films through aerosol deposition. *J. Eur. Ceram. Soc.* **2020**, *40* (1), 63−70.

(32) Park, C.-K.; Lee, S.; Lim, J.-H.; Ryu, J.; Choi, D.; Jeong, D.-Y. Nano-size grains and high density of 65PMN-35PT thick film for high energy storage capacitor. *Ceram. Int.* **2018**, *44* (16), 20111−20114.

(33) Akedo, J. Room Temperature Impact Consolidation (RTIC) of Fine Ceramic Powder by Aerosol Deposition Method and Applications to Microdevices. *J. Therm. Spray Technol.* **2008**, *17* (2), 181−198.

(34) Jeong, C. K.; Cho, S. B.; Han, J. H.; Park, D. Y.; Yang, S.; Park, K.-I.; Ryu, J.; Sohn, H.; Chung, Y.-C.; Lee, K. J. Flexible highly-effective energy harvester via crystallographic and computational control of nanointerfacial morphotropic piezoelectric thin film. *Nano Res.* **2017**, *10* (2), 437−455.

(35) Hwang, G.-T.; Annapureddy, V.; Han, J. H.; Joe, D. J.; Baek, C.; Park, D. Y.; Kim, D. H.; Park, J. H.; Jeong, C. K.; Park, K.-I.; Choi, J.-J.; Kim, D. K.; Ryu, J.; Lee, K. J. Self-Powered Wireless Sensor Node Enabled by an Aerosol-Deposited PZT Flexible Energy Harvester. *Adv. Energy Mater.* **2016**, *6* (13), 1600237.

(36) Park, K.-I.; Son, J. H.; Hwang, G.-T.; Jeong, C. K.; Ryu, J.; Koo, M.; Choi, I.; Lee, S. H.; Byun, M.; Wang, Z. L.; Lee, K. J. Highly-Efficient, Flexible Piezoelectric PZT Thin Film Nanogenerator on Plastic Substrates. *Adv. Mater.* **2014**, *26* (16), 2514−2520.

(37) Chan, K. Y.; Tsang, W. S.; Mak, C. L.; Wong, K. H.; Hui, P. M. Effects of composition of PbTiO$_3$ on optical properties of (1-x)PbMg$_{1/3}$Nb$_{2/3}$O$_3$-xPbTiO$_3$ thin films. *Phys. Rev. B: Condens. Matter Mater. Phys.* **2004**, *69*, 144111.

(38) Park, K. I.; Son, J. H.; Hwang, G. T.; Jeong, C. K.; Ryu, J.; Koo, M.; Choi, I.; Lee, S. H.; Byun, M.; Wang, Z. L.; Lee, K. J. Highly-Efficient, Flexible Piezoelectric PZT Thin Film Nanogenerator on Plastic Substrates. *Adv. Mater.* **2014**, *26* (16), 2514−2520.

(39) Park, J. H.; Lee, H. E.; Jeong, C. K.; Kim, D. H.; Hong, S. K.; Park, K. I.; Lee, K. J. Self-powered flexible electronics beyond thermal limits. *Nano Energy* **2019**, *56*, 531−546.

(40) Cross, L. E. Relaxor ferroelectrics. *Ferroelectrics* **1987**, *76* (1), 241−267.

(41) Kwong, W. Y.; Zhang, W. Y. Electron-beam assisted platinum deposition as a protective layer for FIB and TEM applications. *IEEE* **2005**, 469−471.

(42) Wu, N.; Song, X.; Hou, Y.; Zhu, M.; Wang, C.; Yan, H. Relaxor behavior of (1-x)PbMg$_{1/3}$Nb$_{2/3}$O$_3$-xPbTiO$_3$ ceramics. *Chin. Sci. Bull.* **2009**, *54* (7), 1267.

(43) Wang, Y.; Zhou, X.; Chen, Q.; Chu, B.; Zhang, Q. Recent development of high energy density polymers for dielectric capacitors. *IEEE Trans. Dielectr. Electr. Insul.* **2010**, *17* (4), 1036−1042.

(44) Guo, M.; Jiang, J.; Shen, Z.; Lin, Y.; Nan, C.-W.; Shen, Y. High-Energy-Density Ferroelectric Polymer Nanocomposites for Capacitive Energy Storage: Enhanced Breakdown Strength and Improved Discharge Efficiency. *Mater. Today* **2019**, *29*, 49−67.

(45) Chen, L. M.; Sun, N. N.; Li, Y.; Zhang, Q. W.; Zhang, L. W.; Hao, X. H. Multifunctional antiferroelectric MLCC with high-energy-storage properties and large field-induced strain. *J. Am. Ceram. Soc.* **2018**, *101* (6), 2313−2320.

(46) Li, J.; Shen, Z.; Chen, X.; Yang, S.; Zhou, W.; Wang, M.; Wang, L.; Kou, Q.; Liu, Y.; Li, Q.; Xu, Z.; Chang, Y.; Zhang, S.; Li, F. Grain-orientation-engineered multilayer ceramic capacitors for energy storage applications. *Nat. Mater.* **2020**, *19* (9), 999−1005.

(47) Yang, L.; Kong, X.; Cheng, Z.; Zhang, S. Ultra-high energy storage performance with mitigated polarization saturation in lead-free relaxors. *J. Mater. Chem. A* **2019**, *7* (14), 8573−8580.

(48) Chu, B.; Zhou, X.; Ren, K.; Neese, B.; Lin, M.; Wang, Q.; Bauer, F.; Zhang, Q. M. A Dielectric Polymer with High Electric Energy Density and Fast Discharge Speed. *Science* **2006**, *313* (5785), 334−336.

(49) Hwang, G.-T.; Park, H.; Lee, J.-H.; Oh, S.; Park, K.-I.; Byun, M.; Park, H.; Ahn, G.; Jeong, C. K.; No, K.; Kwon, H.; Lee, S.-G.; Joung, B.; Lee, K. J. Self-Powered Cardiac Pacemaker Enabled by Flexible Single Crystalline PMN-PT Piezoelectric Energy Harvester. *Adv. Mater.* **2014**, *26* (28), 4880−4887.

(50) Kishi, H.; Mizuno, Y.; Chazono, H. Base-Metal Electrode-Multilayer Ceramic Capacitors: Past, Present and Future Perspectives. *Jpn. J. Appl. Phys.* **2003**, *42* (Part 1, No. 1), 1−15.

(51) Park, J. H.; Han, S.; Kim, D.; You, B. K.; Joe, D. J.; Hong, S.; Seo, J.; Kwon, J.; Jeong, C. K.; Park, H.-J.; Kim, T.-S.; Ko, S. H.; Lee, K. J. Plasmonic-Tuned Flash Cu Nanowelding with Ultrafast Photochemical-Reducing and Interlocking on Flexible Plastics. *Adv. Funct. Mater.* **2017**, *27* (29), 1701138.

(52) Kim, S. J.; Choi, H.; Kim, Y.; We, J. H.; Shin, J. S.; Lee, H. E.; Oh, M.-W.; Lee, K. J.; Cho, B. J. Post ionized defect engineering of the screen-printed Bi$_2$Te$_{2.7}$Se$_{0.3}$ thick film for high performance flexible thermoelectric generator. *Nano Energy* **2017**, *31*, 258−263.